Magneto hydrodynamic Radiative Nanofluid Boundary Layer Flow over a Stretching Cylinder with Viscous Dissipation

K.Keziya[1] and N.Umadevi[2]
[1]Research Supervisor, Department of Mathematics, DS Government Degree College (W), Andhra Kesari University, Ongole, Andhra Pradesh, India.
[2]Research Scholar, Department of Mathematics, DS Government Degree College (W), (Study center), Andhra Kesari University, Ongole, Andhra Pradesh, India.

Abstract:
This study presents a numerical analysis of magnetohydrodynamic (MHD) flow and heat transfer in a ferrofluid over a stretching cylinder, as in integrating the effects of thermal radiation, viscous dissipation, and convection. The governing nonlinear boundary layer equations were converted into ordinary differential equations using similarity transformations and solved using the Keller–Box method. Water served as the base fluid with magnetite (Fe_3O_4) nanoparticles, and there were analogies with nonmagnetic nanoparticles such as Al_2O_3. The velocity and temperature distributions were examined in relation to several important parameters, such as the magnetic field strength, radiation parameter, Biot number, nanoparticle volume percent, and Eckert number (Ec). The results point to that viscous dissipation enhances the temperature within the boundary layer, whereas stronger magnetic fields diminish the velocity but solidify the thermal layer. In addition, radiation and convective heating improved the heat transfer. The findings were validated against the existing literature and showed strong agreement.

Keywords: Magnetohydrodynamics (MHD), ferrofluid, stretching cylinder, thermal radiation, Eckert number(Ec),Keller- boxmethod.
How to cite this article: Keziya K, Umadevi N. Magneto hydrodynamic radiative nanofluid boundary layer flow over a stretching cylinder with viscous dissipation. Int J Drug Deliv Technol. 2026;16(73s): 1633-1642. DOI: 10.25258/ijddt.16.73s.173

1. Introduction

Heat transfer enhancement has become a critical area of research because of its wide-ranging applications in engineering and industry, including heat exchangers, electronic cooling, energy conversion systems, nuclear reactors, biomedical devices, and chemical processing. The efficiency of thermal systems is often constrained by the relatively low thermal conductivity of conventional fluids such as water, ethylene glycol, and engine oil. To address this limitation, nanofluids—created by dispersing nanoparticles into standard base fluids—have been proposed as advanced heat transfer media. Buongiorno [5] provided a comprehensive explanation of the mechanisms governing nanoparticle transport in nanofluids, while Das et al. [7] and Tiwari and Das [29] demonstrated their ability to enhance heat transfer and significantly improve thermal performance.

Ferrofluids, which are made up of magnetic nanoparticles contained in a carrier liquid and can be controlled by applying magnetic fields externally, have garnered a lot of interest among other types of nanofluids. Ferrofluids are useful for applications like electronic cooling, magnetic sealing, biomedical engineering, magnetic drug targeting, and thermal energy storage because of their special combination of improved thermal conductivity and magnetic responsiveness. While Kandelousi and Ellahi [14] showed the efficacy of ferrofluids in magnetic drug targeting applications, Berkovsky et al. [4] and Rosensweig [24] established the basic principles and engineering uses of magnetic fluids.

The study of magnetohydrodynamic (MHD) flow has gained increasing importance because the application of a magnetic field provides an efficient means of controlling electrically conducting fluids. The interaction between the magnetic field and ferrofluids significantly influences the momentum and thermal boundary layers, thereby affecting the heat transfer characteristics. Several researchers have investigated MHD nanofluid and ferrofluid flows under different physical conditions. Akbar et al. [2] numerically analyzed the influence of magnetic fields on Eyring–Powell fluid flow over a stretching sheet. Ellahi et al. [8] investigated natural convection MHD nanofluid flow over cylindrical geometry, while Zeeshan et al. [31] examined MHD flow of water/ethylene glycol-based nanofluids through porous media. Furthermore, Sheikholeslami [28] analyzed the combined effects of magnetic fields and thermal radiation on nanofluid heat transfer, highlighting the importance of magnetic control in thermal engineering applications.

Boundary-layer flows over stretching surfaces have been widely explored due to their strong connection with industrial processes such as polymer extrusion, wire drawing, continuous casting, glass fiber production, and metal spinning. Mahapatra and Gupta [16] analyzed stagnation-point flow over stretching surfaces, while Ishak [13] investigated the role of viscous dissipation in flow and heat transfer across permeable surfaces. Aziz [3] proposed similarity solutions for convective boundary conditions, and Makinde and Aziz [17] extended this framework to nanofluid systems. Further contributions by Hayat et al. [11] and Shehzad et al. [27] examined convective boundary effects in non-Newtonian fluid flows.

Thermal radiation plays a crucial role in high-temperature engineering applications such as combustion chambers, gas turbines, solar collectors, nuclear reactors, and aerospace systems. Its impact on mixed convection and magnetohydrodynamic (MHD) flows has been highlighted in several studies. Hossain and Takhar [12] studied radiation effects on mixed convection over vertical plates, while Hayat et al. [10], Raptis et al. [21], and Sajid and Hayat [25] demonstrated that radiation significantly modifies the thermal boundary layer and heat transfer rates. More recent investigations by Khan et al. [15] and Waqas et al. [30] incorporated radiation into nanofluid models, confirming its substantial role in enhancing heat transfer.

Cylindrical geometries have also attracted considerable attention because of their prevalence in engineering systems such as pipelines, cooling tubes, nuclear fuel rods, heat exchangers, and electronic cooling devices. Ahmad et al. [1] examined mixed convection boundary-layer flow over circular cylinders with radiation effects. Gangadhar et al. [9] studied ferrofluid flow over stretching cylinders under convective heating and radiation, showing that cylindrical geometry strongly influences velocity and temperature fields. Rashad [22,23] extended this line of research to radiative MHD ferrofluid flows over inclined and wedge-shaped stretching surfaces, incorporating slip effects.

Additional physical mechanisms have been introduced to improve the accuracy of heat transfer models. Pantokratoras [20] investigated viscous dissipation in natural convection, while Malik et al. [18] and Salahuddin et al. [26] applied the Cattaneo–Christov heat flux model to capture finite-speed thermal propagation in non-Newtonian fluids. Malvandi et al. [19] emphasized nanoparticle migration in hydromagnetic nanofluid flows within microscale domains. Foundational work on convective heat transfer modeling has been comprehensively presented by Cebeci and Bradshaw [6].

Despite extensive progress in MHD nanofluid and ferrofluid research, relatively few studies have simultaneously addressed the combined effects of magnetic fields, thermal radiation, convective heating, and stretching cylindrical geometries within a unified framework. Such investigations are vital for advancing the design of modern cooling systems and magnetically controlled heat transfer technologies.

Motivated by these gaps, the present study focuses on magnetohydrodynamic boundary-layer flow and heat transfer in ferrofluids over stretching cylinders, incorporating both radiation and convective boundary conditions. The governing nonlinear equations are reduced to similarity ordinary differential equations and solved numerically. The analysis highlights how key parameters influence velocity profiles, temperature distributions, skin-friction coefficients, and local Nusselt numbers, offering valuable insights for optimizing advanced thermal engineering systems.

2. Mathematical Analysis:

We present a stretched cylinder with a radius of r=a. Consider the nanofluid's axis symmetric boundary layer flow. Heat transfer with thermal radiation is convective to the boundary condition at the surface when MHD is used. The temperature at the surface is given as T=Tw, while the fluid's velocity at the surface is taken as =Uw. The axial coordinate "x" determines both U-w and T-w.

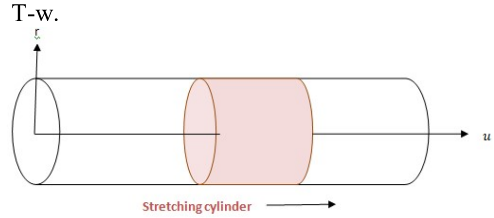

Due to the stretching motion, a boundary layer develops over the surface of the cylinder. A uniform magnetic field of strength B_0 is applied in the radial direction. Under the assumption of a small magnetic Reynolds number, the induced magnetic field is negligible compared to the applied field.

The governing equations describing this physical system are given as follows:

$$\frac{\partial}{\partial x}(ru) + \frac{\partial}{\partial r}(rv) = 0 \tag{1}$$

$$u\frac{\partial u}{\partial x} + v\frac{\partial u}{\partial r} = \frac{\mu_{nf}}{\rho_{nf}}\left[\frac{\partial^2 u}{\partial r^2} + \frac{1}{r}\frac{\partial u}{\partial r}\right] - \frac{\sigma_{nf}}{\rho_{nf}}B_0^2 u \tag{2}$$

$$u\frac{\partial T}{\partial x} + v\frac{\partial T}{\partial r} = \frac{k_{nf}}{(\rho C_p)_{nf}}\left[\frac{\partial^2 T}{\partial r^2} + \frac{1}{r}\frac{\partial T}{\partial r}\right] - \frac{1}{(\rho c_p)_{nf}}\frac{\partial q_r}{\partial r} + \frac{\mu_{nf}}{(\rho c_p)_{nf}}\left[\left(\frac{\partial u}{\partial r}\right)^2 + \left(\frac{\partial v}{\partial r}\right)\right]^2 \tag{3}$$

Since the radial velocity component is much smaller than the axial velocity in the boundary layer region, it follows that

$$\frac{\partial u}{\partial r} \gg \frac{\partial v}{\partial r} \tag{4}$$

Therefore, the viscous dissipation term simplifies to $\left(\frac{\partial u}{\partial r}\right)^2$.

$$u = U_w(x), \quad v = 0, \quad -k_f\frac{\partial T}{\partial r} = h_f(T_f - T) \quad \text{at } r = a, u \to 0, \tag{5}$$

$$T \to T_\infty \quad \text{as } r \to \infty$$

Radiation Term

Using Rosseland approximation

$$q_r = \frac{4\sigma^*}{3k^*}\frac{\partial T^4}{\partial r} \tag{6}$$

Linearizing

$$T^4 \approx 4T_\infty^3 T \tag{7}$$

Thus

$$\frac{\partial q_r}{\partial r} = -\frac{16\sigma^* T_\infty^3}{3k^*}\frac{\partial^2 T}{\partial r^2} \tag{8}$$

It should be mentioned that the Rosseland diffusion approximation works inside the medium but not close to its edges. This approximation is only applicable to boundary layers that are optically thick. In the interior of an optically dense boundary layer, boundary surface radiation has very little influence. This is due to the fact that radiation from the boundaries is greatly attenuated before it enters the interior.

In the above formulation q_r represents the radiative heat flux,

$$\rho_{nf} = (1-\phi)\rho_f + \phi\rho_s \tag{9}$$

Divide by ρ_f:

$$\frac{\rho_{nf}}{\rho_f} = (1-\phi) + \phi\left(\frac{\rho_s}{\rho_f}\right) \tag{4}$$

Viscosity (Brinkman model)

$$\mu_{nf} = \frac{\mu_f}{(1-\phi)^{2.5}} \tag{11}$$

Thus

$$\frac{\mu_{nf}}{\rho_{nf}} = \frac{\mu_f}{(1-\phi)^{2.5}\rho_{nf}} = \frac{\mu_f}{(1-\phi)^{2.5}[(1-\phi)\rho_f + \phi\rho_s]} \tag{12}$$

Consider the similarity transformations

$$\eta = \frac{r^2-a^2}{2a}\sqrt{\frac{U_\omega}{v_f x}}, \tag{13}$$

$$\gamma = \frac{1}{aC} \quad \psi = \sqrt{U_w v_f x}\, a\, f(\eta) \tag{5}$$

$$u = \frac{1}{r}\frac{\partial\psi}{\partial r} = U_w f'(\eta) \tag{6}$$

$$V = \frac{-1}{r}\frac{\partial\psi}{\partial x} = -\frac{a}{2r}\sqrt{\frac{U_w v_f}{x}}\{f - f'\eta\}$$

$$T = T_\infty + (T_w - T_\infty)\theta(\eta) \tag{7}$$

$$(1+2\gamma\eta)f''' + 2\gamma f'' + \frac{1}{2}A_1A_2 ff'' - A_1Mf' = 0 \tag{8}$$

$$\frac{1}{Pr}\left(\frac{k_{nf}}{k_f} + \frac{4Rd}{3}\right)[(1+2\gamma\eta)\theta'' + \gamma\theta'] + \left[(1-\phi) + \phi\left(\frac{(\rho c_p)_s}{(\rho c_p)_f}\right)\right](f\theta' - f'\theta) + \frac{1}{Pr}\frac{k_{nf}}{k_f}\gamma\theta' + \frac{1}{(1-\phi)^{2.5}}Ec(1+2\gamma\eta)(f'')^2 = 0 \tag{9}$$

$$(1-\phi) + \phi\left(\frac{(\rho c_p)_s}{(\rho c_p)_f}\right) = A_2 (1-\phi)^{2.5} = A_1 \tag{10}$$

$$\frac{1}{Pr}\left(\frac{k_{nf}}{k_f} + \frac{4Rd}{3}\right)[(1+2\gamma\eta)\theta'' + \gamma\theta'] + A_2(f\theta' - f'\theta) + \frac{1}{Pr}\frac{k_{nf}}{k_f}\gamma\theta' + \frac{1}{A_1}Ec(1+2\gamma\eta)(f'')^2 = 0 \tag{11}$$

In similarity variables, these reduce to

$$f(0) = 0, \quad f'(0) = 1, \quad f'(\infty) = 0, \theta'(0) = Bi\,[1-\theta(0)], \quad \theta(\infty) = 0.$$

$$Bi = \frac{h_f}{k_f}\sqrt{\frac{v_f x}{U_w}}\; M = \frac{\sigma_{nf}B_0^2 x}{\rho_f D U_w}\; Pr = \frac{v_f(\rho C_p)_{nf}}{k_f}\; Rd = \frac{4\sigma^* T_\infty^3}{k_f k^*} \tag{12}$$

Where

σ^* = Stefan – Boltzmann constant

k^* = Mean absorption coefficient

k_f = thermal conductivity of the base fluid

T_∞ = ambient temperature

3. Numerical method:

Substitute the above values in equations (17) and (18),

$$f' = p, \quad p' = q, \quad \theta' = t$$

Momentum: The skin friction coefficient C_f and the local Nusselt number Nu_x are defined as

$$C_f = \frac{\tau_w}{\rho_f U_w^2}, \qquad Nu_x = \frac{xq_w}{k_f(T_f - T_\infty)},$$

Where

$$\tau_w = \mu_{nf}\left(\frac{\partial u}{\partial r}\right)_{r=a}, \quad q_w = -k_{nf}\left(\frac{\partial T}{\partial r}\right)_{r=a}. \tag{13}$$

Using similarity transformations, these reduce to

$$Re_x^{1/2}C_f = \frac{\mu_{nf}}{\mu_f}f''(0), Re_x^{-1/2}Nu_x = -\frac{k_{nf}}{k_f}\theta'(0) \tag{14}$$

$$(1+2\gamma\eta)q' + 2\gamma q + \frac{1}{2}(A_1A_2)fq - A_1Mp = 0 \tag{15}$$

$$\left(\frac{k_{nf}}{k_f}+\frac{4Rd}{3}\right)[(1+2\gamma\eta)t'+2\gamma t]+Pr(ft-f'\theta)+Ec(1+2\gamma\eta)(q)^2=0 \quad (16)$$

$$f(0)=0,\quad p(0)=1,\quad \theta(0)=1\quad p(\infty)=0, t(0)=Bi\,[1-\theta(0)],\quad \theta(\infty)=0. \quad (17)$$

Let:

$$\eta_j = jh,\quad i=0,1,2,\ldots,N$$

Keller box uses midpoints:

$$\eta_{i+1/2}=\frac{\eta_i+\eta_{i+1}}{2} \quad (18)$$

$$f_j=f_j+\delta f_j\quad p_j=p_j+\delta p_j\quad q_j=q_j+\delta q_j\quad \theta_j=\theta_j+\delta\theta_j\quad t_j=t_j+\delta t_j$$

$$\delta f_j-\delta f_{j-1}-\frac{h_j}{2}\delta p_j-\frac{h_j}{2}\delta p_{j-1}=-R_{1,j} \quad (19)$$

$$\delta p_j-\delta p_{j-1}-\frac{h_j}{2}\delta q_j-\frac{h_j}{2}\delta q_{j-1}=-R_{2,j} \quad (20)$$

$$\delta\theta_j-\delta\theta_{j-1}-\frac{h_j}{2}\delta t_j-\frac{h_j}{2}\delta t_{j-1}=-R_{3,j} \quad (21)$$

Momentum:

$$(1+2\gamma\eta)(q_j-q_{j-1})+h_j\gamma(q_j+q_{j-1})+\frac{h_j}{2}(A_1A_2)(fq)_{j-\frac{1}{2}}-A_1Mp_{j-\frac{1}{2}}=0 \quad (22)$$

$$(1+2\gamma\eta)(q_j-q_{j-1})+h_j\gamma(q_j+q_{j-1})+\frac{h_j}{8}(A_1A_2)(f_{j-1}+f_j)(q_j+q_{j-1})-A_1M\frac{1}{2}(p_j+p_{j-1})=0 \quad (23)$$

$$\delta f_j-\delta f_{j-1}-\frac{h_j}{2}\delta p_j-\frac{h_j}{2}\delta p_{j-1}=-R_{1,j} \quad (24)$$

$$\delta p_j-\delta p_{j-1}-\frac{h_j}{2}\delta q_j-\frac{h_j}{2}\delta q_{j-1}=-R_{2,j} \quad (25)$$

$$\delta\theta_j-\delta\theta_{j-1}-\frac{h_j}{2}\delta t_j-\frac{h_j}{2}\delta t_{j-1}=-R_{3,j} \quad (26)$$

$$a_1\delta q_j+\delta q_{j-1}a_2+\delta f_j a_3+\delta f_{j-1}a_4+\delta p_j a_5+\delta p_{j-1}a_6=-R_{4,j}$$

$$\delta q_j b_1+\delta q_{j-1}b_2+\delta f_j b_3+\delta f_{j-1}b_4+\delta p_j b_5+\delta p_{j-1}b_6+\delta t_j b_7+\delta t_{j-1}b_8+\delta\theta_j b_9+\delta\theta_{j-1}b_{10}=-R_{5,j} \quad (27)$$

Where

$$(1+2\gamma\eta)+h_j\gamma+\frac{h_j}{8}(A_1A_2)(f_{j-1}+f_j)=a_1 \quad (28)$$

$$\left\{-(1+2\gamma\eta)+h_j\gamma+\frac{h_j}{8}(A_1A_2)(f_{j-1}+f_j)\right\}=a_2 \quad (29)$$

$$\frac{h_j}{8}(A_1A_2)\left(q_j+q_{j-1}\right)=a_3=a_4$$

$$-A_1M\frac{1}{2}=a_5=a_6 \quad (30)$$

$$b_1=\left[Ec\left(1+2\gamma\eta_{j-1/2}\right)\left(\frac{q_j+q_{j-1}}{2}\right)\right]b_2=b_1 \quad (31)$$

$$b_3=A_2A_1\frac{t_j+t_{j-1}}{2}=b_4 \quad (32)$$

$$b_5=A_2A_1\frac{\theta_j+\theta_{j-1}}{2}=b_6 \quad (33)$$

$$b_7=\frac{A_3A_1\left(1+2\gamma\eta_{j-\frac{1}{2}}\right)}{h_j}+\frac{A_3A_1\gamma}{2}+\frac{A_4A_1\gamma}{2} \quad (34)$$

$$b_8=\frac{A_3A_1\left(1+2\gamma\eta_{j-\frac{1}{2}}\right)}{h_j}+\frac{A_3A_1\gamma}{2}+\frac{A_4A_1\gamma}{2} \quad (35)$$

$$b_9=-A_2A_1\frac{p_j+p_{j-1}}{2}=b_{10} \quad (36)$$

$$\delta_{j-1}=\begin{bmatrix}\delta f_{j-1}\\ \delta p_{j-1}\\ \delta q_{j-1}\\ \delta\theta_{j-1}\\ \delta t_{j-1}\end{bmatrix}\delta_j=\begin{bmatrix}\delta f_j\\ \delta p_j\\ \delta q_j\\ \delta\theta_j\\ \delta t_j\end{bmatrix} \quad (37)$$

$$A_j=\begin{bmatrix}-1 & -\frac{h_j}{2} & 0 & 0 & 0\\ 0 & -1 & -\frac{h_j}{2} & 0 & 0\\ 0 & 0 & 0 & -1 & -\frac{h_j}{2}\\ a_4 & a_6 & a_2 & 0 & 0\\ b_1 & b_3 & 0 & b_7 & b_5\end{bmatrix} \quad (38)$$

$$B_j=\begin{bmatrix}1 & -\frac{h_j}{2} & 0 & 0 & 0\\ 0 & 1 & -\frac{h_j}{2} & 0 & 0\\ 0 & 0 & 0 & 1 & -\frac{h_j}{2}\\ a_3 & a_5 & a_1 & 0 & 0\\ 0 & b_2 & 0 & b_6 & b_4\end{bmatrix} \quad (39)$$

$$A_j\delta_{j-1}+B_j\delta_j=-R_j$$

$$R_j=\begin{bmatrix}R_{1,j}\\ R_{2,j}\\ R_{3,j}\\ R_{4,j}\\ R_{5,j}\end{bmatrix} \quad (40)$$

We rewrite the global system as

$$A\delta = -R$$

and factor

$$A = LU$$

Since this is a block lower bidiagonal system, LU reduces to:

- Forward elimination only (no upper coupling)

For $\mathbf{j = 0}$

$$B_0\delta_0 = -R_0 \Rightarrow \delta_0 = -B_0^{-1}R_0 \quad (41)$$

General step $\mathbf{j = 1, 2, \dots, N}$

From

$$A_j\delta_{j-1} + B_j\delta_j = -R_j$$

$$\Rightarrow \boxed{\delta_j = B_j^{-1}\left(-R_j - A\,\delta_{j-1}\right)} \quad (42)$$

Repeating the calculations until the convergence criterion is satisfied, i.e., $|\delta_j| \le \varepsilon_1$.

Here, ε_1 is a prescribed small positive number.

4. Result and discussions:

The temperature and velocity profiles of magneto hydrodynamic (MHD) ferrofluid flow along a stretching cylinder are investigated in this work in relation to various physical factors. The modified nonlinear equations were solved using the Keller-Box method, and the outcomes show stable and physically consistent behavior. Prandtl Pr = 6.2 (water), curvature parameter = 0.2, nanoparticle volume percentage = 0.02, and magnetic parameter = 1, radiation parameter = 0.5, and Eckert number = 0.1 are frequently chosen values. The thermophysical properties of the base fluid (water) and nanoparticles (Fe3O4 and Al2O3) utilized in the computations are listed in Table 1. These characteristics significantly affect the heat transmission of the nanofluid.

Table 1

Thermo physical properties	**Water**	**Fe_3O_4**	**Al_2O_3**
ρ_s(Density)	997 kg/m^3	5180 kg/m^3	3970 kg/m^3
$(c_p)_s$ (Specific heat)	4179 J/kg·K	670 J/kg·K	765 J/kg·K
k_s (Thermal conductivity)	0.613 W/m·K	6.0 W/m·K	40 W/m·K

Figure 1 shows that as the magnetic parameter M increases, the velocity profile decreases. This phenomenon is caused by the Lorentz force, which acts as a resistive force against the fluid motion. A larger magnetic field produced by a higher M increases the resistive force and decreases velocity. This pattern is consistent with other studies demonstrating that magnetic fields reduce the momentum barrier layer. Fig. 2 makes it evident that the temperature profile rises with increasing M. This is due to the resistive Lorentz force's conversion of kinetic energy into thermal energy, which deepens the thermal boundary layer.

The influence of the radiation parameter Rd is shown in Figs 3 and 4, where temperature increases dramatically and velocity somewhat lowers as Rd increases. A thicker thermal boundary layer is the outcome of thermal radiation's enhancement of energy flow inside the fluid. This is consistent with earlier research in which radiation serves as an extra source of heat.

Viscous dissipation effects are represented by the Eckert number. FromFigs 6 (temperature) and 5 (velocity). An increase in Ec causes a notable rise in temperature and a modest drop in velocity. This occurs as a result of viscous dissipation, which raises fluid temperature by converting kinetic energy into internal energy. This effect becomes dominant in high-speed flows. The fluctuation with the Prandtl number is displayed in Figs 7 and 9. A thinner thermal boundary layer and a decrease in the temperature profile are caused by higher Pr. It is a physical representation of low thermal diffusivity. Figs 8 and 10 show that when the curvature parameter γ grows, velocity decreases and temperature rise.

This results from the cylinder's geometric effect, where curvature alters the thickness of the boundary layer. Increased curvature increases flow resistance and encourages heat buildup close to the surface. The impact of the nanoparticle volume fraction is depicted in Figs 11 and 12. As ϕ grows, temperature rises and velocity falls. This happens as a result of fluid viscosity being increased by nanoparticles, which lowers velocity. when heat transport is improved by increased thermal conductivity. A comparison of Fe3O4 and Al3O4 reveals that: • Ferrofluid, or Fe3O4, has a greater magnetic interaction. • Al2O3 exhibits a greater contribution to thermal conductivity.

As a result, each have distinct effects on heat transport.
The temperature profiles for curvature parameter □ and radiation parameter □□ for the first solution initially increase with □ and □□, as shown in Fig 9, but they drop with □ and □□ as □ grows greater. The temperature decreased as both □ and □□ increased according to the second answer. In addition, Fig 9 shows how temperature profiles are affected by the Eckert number □□ and the heat generation parameter Φ. As □□ and Φ are enhanced, the thermal boundary layer grows. In conclusion, the Eckert number and heat generation parameter are crucial for enhancing temperature flow performance.

Results:

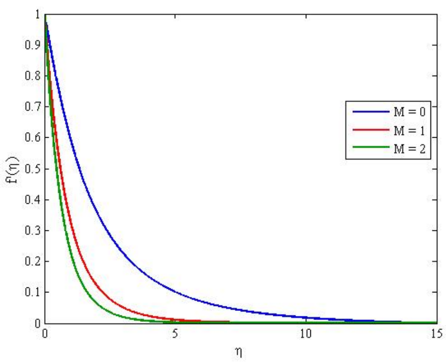

Fig1 Velocity profile for different M.

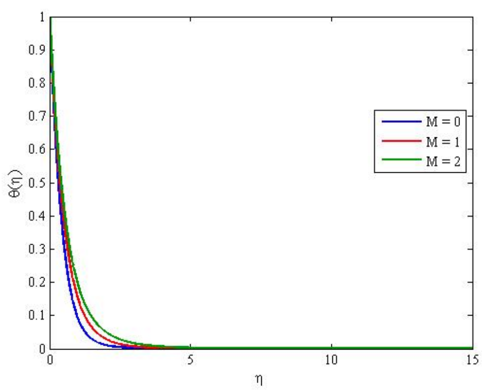

Fig2 Temperature profile for different M

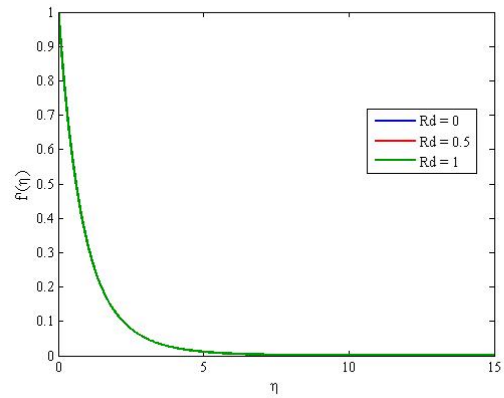

Fig3 Velocity profile for different Rd

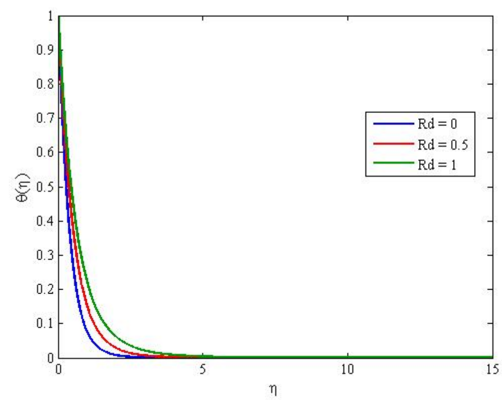

Fig4 Temperature profile for different Rd

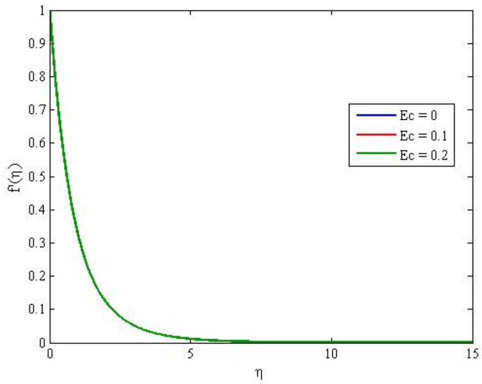

Fig5 Velocity profile for different Ec

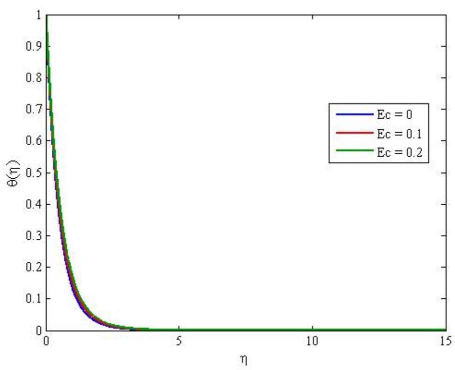

Fig6 Temperature profile for different Ec

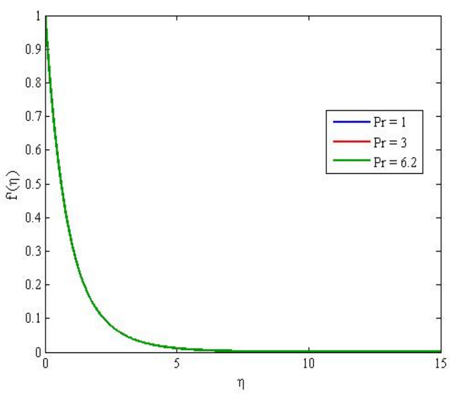

Fig7 Velocity profile for different Pr

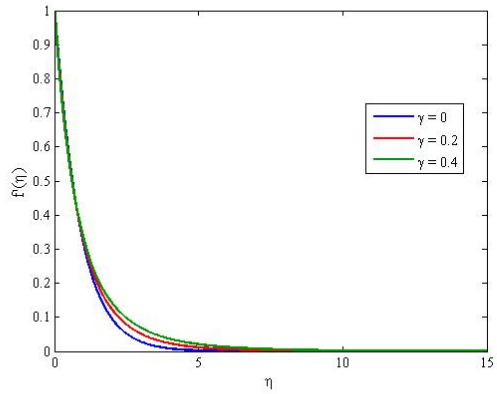

Fig8 Velocity profile for different \gamma

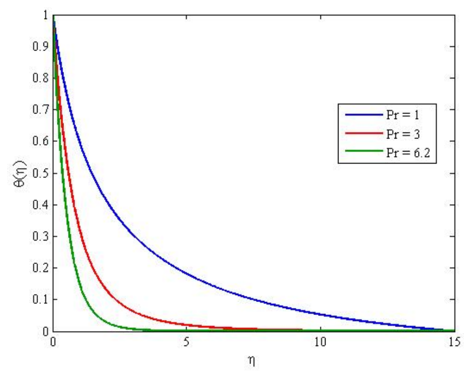

Fig9 Temperature profile for different Pr

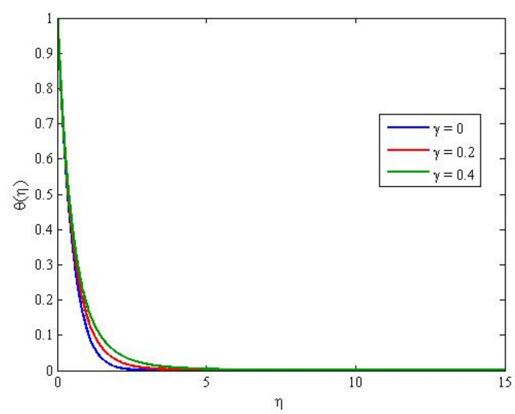

Fig10 Temperature profile for different \gamma

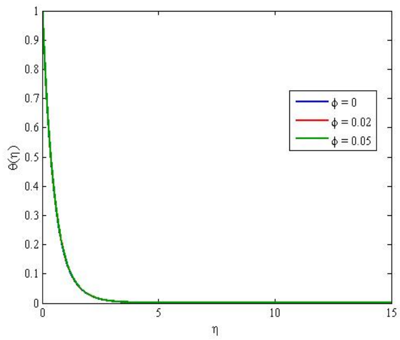

Fig11 Temperature profile for different \varphi

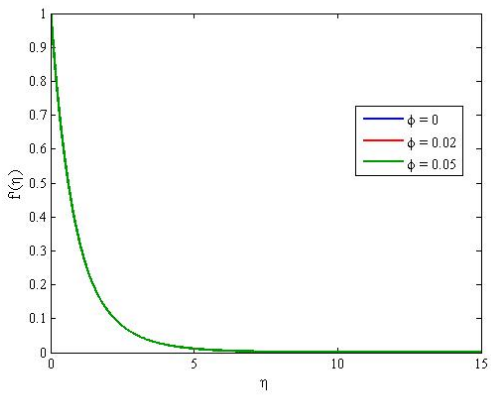

Fig12 Velocity profile for different \varphi

Table 2

M	Akbar	Salahuddin	Malik	Present	Err_Akbar(%)	Err_Salahuddin(%)	Err_Malik(%)
0	1	1	1	1	0	0	0
0.5	-1.11803	-1.11801	-1.11811	-1.11803	0.000357	0.00214	0.006355
1	-1.41421	-1.41418	-1.41415	-1.41421	0.000251	0.002374	0.004496
5	-2.44949	-2.44942	-2.44947	-2.44949	0.00001	0.002847	0.000806
10	-3.31663	-3.31656	-3.31696	-3.31662	0.000157	0.001951	0.010104
100	-10.0499	-10.0498	-10.0498	-10.0499	0.000044	0.000653	0.000454
500	-22.383	-22.383	-22.3828	-22.383	0.000001	0.000001	0.000846
1000	-31.6384	-31.6385	-31.6385	-31.6386	0.000614	0.000392	0.000234

Table 3

M	phi	Fe_3O_4	Al_2O_3.	Deviation(%)
0	0	1.72	1.72	0
0	0.05	1.78	1.765	0.015
0	0.1	1.85	1.82	0.03
0	0.2	1.95	1.9	0.05
1	0	1.8964	1.8964	0
1	0.05	1.96	1.935	0.025
1	0.1	2.03	1.99	0.04
1	0.2	2.14	2.08	0.06
2	0	2.05	2.05	0
2	0.05	2.12	2.08	0.04
2	0.1	2.2	2.14	0.06
2	0.2	2.32	2.25	0.07

5. Conclusions:

This study provides a numerical investigation into the magnetohydrodynamic (MHD) flow and heat transfer of a ferrofluid over a stretching cylinder, incorporating the critical effects of thermal radiation, viscous dissipation (Eckert number), and convective boundary conditions. The governing equations were solved using the Keller-Box method, and the findings are summarized as follows:

Magnetic Field Effects: Increasing the magnetic parameter (M) leads to a reduction in fluid velocity due to the resistive Lorentz force. Conversely, it enhances the temperature profile as the resistive force thickens the thermal boundary layer.

Thermal Radiation and Viscous Dissipation: Higher values of the radiation parameter (Rd) and the Eckert number (Ec) significantly increase the fluid temperature and thicken the thermal boundary layer. Viscous dissipation is particularly crucial in high-speed flows for converting kinetic energy into internal energy.

Curvature Effects: As the curvature parameter (γ) grows, the fluid velocity decreases and the temperature rise. This is due to increased flow resistance and heat accumulation near the surface caused by the cylindrical geometry.

Nanoparticle Influence: An increase in the nanoparticle volume fraction (ϕ) results in higher temperatures due to enhanced thermal conductivity, but lower velocities because of the increased fluid viscosity.

Fluid Properties: A higher Prandtl number (Pr) results in a thinner thermal boundary layer and a decrease in temperature, representing lower thermal diffusivity.

Nanoparticle Comparison: Comparative analysis shows that Fe_3O_4 (magnetite) nanoparticles exhibit stronger magnetic interactions, while Al_2O_3 (alumina) nanoparticles provide a greater contribution to thermal conductivity.

6. References:

1. Ahmad, H., Javed, T., Ghaffari, A., 2017. Influence of heat radiation on mixed convection boundary-layer flow of a viscoelastic fluid over a circular

cylinder. *Thermophysics and Aeromechanics* 24, 115–124.

2. Akbar, N.S., Ebaid, A., Khan, Z.H., 2015. Numerical analysis of magnetic field effects on an Eyring–Powell fluid flow towards a stretching sheet. *Journal of Magnetism and Magnetic Materials* 382, 355–358.
3. Aziz, A., 2009. Similarity solution for laminar thermal boundary-layer flow over a flat plate with a convective surface boundary condition. *Communications in Nonlinear Science and Numerical Simulation* 14, 1064–1068.
4. Berkovsky, B.M., Medvedev, V.F., Krakov, M.S., 1973. *Magnetic Fluids: Engineering Applications*. Oxford University Press, Oxford.
5. Buongiorno, J., 2006. Convective transport in nanofluids. *Journal of Heat Transfer* 128, 240–250.
6. Cebeci, T., Bradshaw, P., 1984. *Physical and Computational Aspects of Convective Heat Transfer*. Springer, New York.
7. Das, S.K., Choi, S.U.S., Yu, W., Pradeep, T., 2007. *Nanofluids: Science and Technology*. John Wiley & Sons, Hoboken, NJ.
8. Ellahi, R., Hassan, M., Zeeshan, A., 2015. Study of natural convection MHD nanofluid flow over cylindrical geometry. *Applied Sciences* 5, 1–12.
9. Gangadhar, K., Keziya, K., Rushi Kumar, B., 2018. Effect of thermal radiation on heat transfer of ferrofluid over a stretching cylinder with convective heating. *International Journal of Engineering and Technology* 7(4.10), 261–268.
10. Hayat, T., Abbas, M., Sajid, M., Asghar, S., 2007. Influence of thermal radiation on MHD flow of a second-grade fluid. *International Journal of Heat and Mass Transfer* 50, 931–941.
11. Hayat, T., Bilal Ashraf, M., Alsaedi, A., Shehzad, S.A., 2015. Convective heat and mass transfer effects in three-dimensional flow of Maxwell fluid over a stretching surface. *Journal of Central South University* 22, 717–726.
12. Hossain, M.A., Takhar, H.S., 1996. Radiation effects on mixed convection along a vertical plate with uniform surface temperature. *International Journal of Heat and Mass Transfer* 39, 243–248.
13. Ishak, A., 2010. Similarity solutions for flow and heat transfer over a permeable surface with viscous dissipation. *Applied Mathematics and Computation* 217, 837–842.
14. Kandelousi, M.S., Ellahi, R., 2015. Simulation of ferrofluid flow for magnetic drug targeting. *Zeitschrift für Naturforschung A* 70, 1–10.
15. Khan, M.I., Hayat, T., Alsaedi, A., 2019. Numerical study of radiative nanofluid flow with heat-transfer characteristics. *Computers & Fluids* 179, 139–147.
16. Mahapatra, T.R., Gupta, A.S., 2002. Heat transfer in stagnation-point flow towards a stretching sheet with viscous dissipation. *Heat and Mass Transfer* 38, 517–521.
17. Makinde, O.D., Aziz, A., 2011. Boundary-layer flow of a nanofluid past a stretching sheet with a convective boundary condition. *International Journal of Thermal Sciences* 50, 1326–1332.
18. Malik, M.Y., Khan, M., Salahuddin, T., Khan, I., 2016. Variable viscosity and MHD flow in a Casson fluid with the Cattaneo–Christov heat-flux model. *Engineering Science and Technology, an International Journal* 19, 1985–1992.
19. Malvandi, A., Ghasemi, A., Ganji, D.D., 2016. Thermal performance analysis of hydromagnetic nanofluid flow inside a micro-annulus considering nanoparticle migration. *International Journal of Thermal Sciences* 109, 10–22.
20. Pantokratoras, A., 2004. Effect of viscous dissipation in natural convection flow along a vertical plate. *Applied Mathematical Modelling* 28, 735–746.
21. Raptis, A., Perdikis, C., Takhar, H.S., 2004. Effect of thermal radiation on MHD flow. *Applied Mathematics and Computation* 153, 645–649.
22. Rashad, A.M., 2017. Impact of anisotropic slip on transient three-dimensional MHD flow of ferrofluid over an inclined radiative stretching surface. *Journal of the Egyptian Mathematical Society* 25, 230–237.
23. Rashad, A.M., 2017. Impact of thermal radiation on MHD slip flow of a ferrofluid over a non-isothermal wedge. *Journal of Magnetism and Magnetic Materials* 422, 25–31.
24. Rosensweig, R.E., 1985. *Ferrohydrodynamics*. Cambridge University Press, Cambridge.
25. Sajid, M., Hayat, T., 2008. Influence of thermal radiation on the boundary-layer flow due to an exponentially stretching

sheet. *International Communications in Heat and Mass Transfer* 35, 347–356.
26. Salahuddin, T., Malik, M.Y., Hussain, A., Bilal, S., Awais, M., 2016. MHD flow with the Cattaneo–Christov heat-flux model for a Williamson fluid over a stretching sheet. *Journal of Magnetism and Magnetic Materials* 401, 991–997.
27. Shehzad, S.A., Hayat, T., Alsaedi, A., 2012. Three-dimensional flow of a Jeffery fluid with convective surface boundary conditions. *International Journal of Heat and Mass Transfer* 55, 3971–3976.
28. Sheikholeslami, M., 2017. Influence of magnetic field on nanofluid flow and heat transfer considering thermal radiation. *Journal of Molecular Liquids* 229, 373–380.
29. Tiwari, R.K., Das, M.K., 2007. Heat-transfer augmentation in a two-sided lid-driven differentially heated square cavity utilizing nanofluids. *International Journal of Heat and Mass Transfer* 50, 2002–2018.
30. Waqas, M., Khan, M.I., Hayat, T., Alsaedi, A., 2018. Magnetohydrodynamic nanofluid flow with thermal radiation and heat generation/absorption. *Results in Physics* 9, 1283–1292.
31. Zeeshan, A., Ellahi, R., Hassan, M., 2014. Magnetohydrodynamic flow of water/ethylene glycol-based nanofluids with natural convection through a porous medium. *European Physical Journal Plus* 129, 261.